HHS Public Access

Author manuscript

J Am Chem Soc. Author manuscript; available in PMC 2017 July 21.

Published in final edited form as:

J Am Chem Soc. 2014 November 05; 136(44): 15631–15637. doi:10.1021/ja507812v.

MD simulations identify time scale of conformational changes responsible for conformational selection in molecular recognition of HIV-1 TAR RNA

Francesco Musiani[†,‡,§,#], **Giulia Rossetti**[§,∥,#], **Luciana Capece**[∇,⊥], **Thomas Martin Gerger**[§], **Cristian Micheletti**[†], **Gabriele Varani**[○,*], and **Paolo Carloni**[§,*]

[†]Scuola Internazionale Superiore di Studi Avanzati (SISSA/ISAS), via Bonomea 265, 34136 Trieste, Italy

[‡]Laboratory of Bioinorganic Chemistry, Department of Pharmacy and Biotechnology, University of Bologna, 40127 Bologna, Italy

[§]Institute of Neuroscience and Medicine INM-9 and Computational Biomedicine, Institute for Advanced Simulation IAS-5 and Computational Biophysics, German Research School for Simulation Sciences, Forschungszentrum Jülich, 52425 Jülich, Germany

[∥]Jülich Supercomputing Centre, Forschungszentrum Jülich, 52425 Jülich, Germany

[∇]International Centre for Genetic Engineering and Biotechnology, AREA Science Park, Padriciano 99, 34149 Trieste, Italy

[○]Department of Chemistry and Department of Biochemistry, University of Washington, Seattle, 98195 WA, USA

Abstract

The HIV-1 Tat protein and several small molecules bind to HIV-1 Trans-Activation Responsive RNA (TAR) by selecting sparsely populated but pre-existing conformations. Thus, a complete characterization of TAR conformational ensemble and dynamics is crucial to understand this paradigmatic system and could facilitate the discovery of new anti-virals targeting this essential regulatory element. We show here that molecular dynamics simulations can be effectively used towards this goal by bridging the gap between functionally-relevant timescales that are inaccessible to current experimental techniques. Specifically, we have performed several independent microsecond long molecular simulations of TAR based on one of the most advanced force fields available for RNA, the parmbsc0 AMBER. Our simulations are first validated against available experimental data, yielding an excellent agreement with measured residual dipolar

[*]**Corresponding Authors**. GV: varani@chem.washington.edu, PC: p.carloni@grs-sim.de.

[⊥]**Present Addresses**

Departamento de Química Biológica-CONICET / Departamento de Química Inorgánica, Analítica y Química Física, Facultad de Ciencias Exactas y Naturales, Universidad de Buenos Aires, C1428EHA, Buenos Aires, Argentina.

[#]These authors contributed equally.

ASSOCIATED CONTENT

Supporting Information. Complete methods, tables S1–S3 and Figures S1–S20. This material is available free of charge via the Internet at http://pubs.acs.org.

Author Contributions

The manuscript was written through contributions of all authors. All authors have given approval to the final version of the manuscript.

couplings and order parameter S^2. This contrast with previous MD simulations (Salmon *et al., J. Am. Chem. Soc.* **2013** 135, 5457–5466) based on the CHARMM36 force field, which could achieve only modest accord with the experimental RDC values. Next, we direct the computation towards characterizing the internal dynamics of TAR over the microsecond timescale. We show that the conformational fluctuations observed over this previously-elusive timescale have a strong functionally-oriented character in that they are primed to sustain and assist ligand binding.

Graphical Abstract

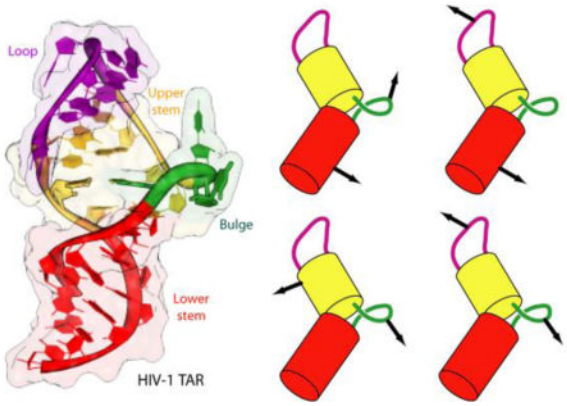

Keywords

HIV-1; Trans-Activation Responsive RNA; Molecular Dynamics; Conformational Selection

INTRODUCTION

The growing number of newly discovered noncoding RNAs raises the demand to explore and characterize their distinct roles in cells.[1–3] An emerging theme is that RNA's functional complexity is rooted not only in its 3D structure but also in its ability to adaptively acquire very distinct conformations on its own or in response to specific cellular signals.[4]

A paradigmatic case of complex and multilayer RNA dynamics is provided by the HIV-1 Trans-Activation Responsive RNA (TAR). TAR is a 59-nucleotide long RNA located at the 5'-end of viral transcripts.[5] It activates elongation of transcription of the integrated virus[6] by forming a complex with the virally encoded HIV-1 Tat protein[7–9] and with human cyclin T1, which recruits the kinase activity of p-TEFb to the HIV-1 promoter. Since viral replication is disrupted by mutations that disfavor the interaction between TAR and its protein partners,[10] the identification of compounds that interact with TAR and prevent formation of the complex with p-TEFb could provide antiviral leads with radically new mechanism of action.[10–12]

NMR studies[13–21] have established that TAR binds to Tat mimics and small ligands mostly through its "bulge" and the neighboring base pairs, consisting of single stranded nucleotides (NTs) 23–25 separating two helical regions ("upper" and "lower" stems, Fig. 1). In *apo* TAR, the partial stacking of U23 on A22 and C24 on U23 in the bulge generates a kink

between the two stems (Fig. 1).[14] Most ligand-bound complexes (referred to as *holo* TAR here) overlap with such *apo* conformation. Few ligands widen instead the major groove and open up the interhelical angle (Tab. S1).[15–17] Hence, ligands binding to TAR can "grab on the fly" a matching TAR conformer as it is spontaneously, yet transiently populated in free TAR,[22] suggesting that such ligands use the conformational selection mechanisms for molecular recognition of TAR (Tab. S1).[13,18–21]

In order to understand TAR/ligand recognition mechanism, an in-depth characterization of the internal motions of this RNA is necessary,[23–25] including an understanding of the interplay among relevant time scales. Conformational exchange in TAR has been shown to occur over a very wide range of rates, from ps to ms. As a consequence of this breadth of motional rates, probing experimentally the mechanism of recognition is very challenging.[26–28] On the one hand, the insight provided by NMR in the solution state (solNMR) is limited by the paucity of observables[22] as well as by technical difficulties in accessing the ns-μs time scale; residual dipolar couplings can access this motional time scale but the information on rates of motion is lost by averaging and can only be obtained partially and indirectly. On the other hand, solid state NMR (ssNMR) can access this time scale, but the information that can be obtained so far by this approach is limited to relatively few sites that have to be probed individually.

Atomistic molecular dynamics (MD) simulations can obviously complement experimental investigations if they are accurate. These approaches, including the recent multi-μs simulation of *apo* TAR[28] based on the CHARMM36 force field,[30–32] have provided valuable support for the conformational-selection mechanism to explain the interaction between TAR and other ligands. Yet the scope of unbiased atomistic MD simulations in addressing RNA dynamics has been much more limited so far than for proteins, due to imperfections of the parameterizations of the atomistic force field for nucleic acids.[33–36] In the case of TAR, the latter shortcoming, along with the challenges posed by extensive conformational sampling, might be responsible for the modest agreement previously reported for residual dipolar couplings (RDCs) calculated from MD simulations and those observed experimentally.[28] Fortunately, recent breakthroughs in force field parameterization indicate that MD simulations of RNA molecules can now be conducted with predictive power. Notably, the latest release of the AMBER force field can accurately reproduce with sub-μs timescale simulations, the structure and conformation of nucleic acids, including, as benchmarks, TAR complexes.[37–39]

Here, we build on these technical advances to re-examine the conformational selection hypothesis of TAR-ligand recognition by using advanced computational techniques to reexamine the experimental results. We collected μs-long MD simulations starting from various instances of *apo* and *holo* TAR structures depleted of the ligands using the parmbsc0 AMBER force field.[37] The viability and effectiveness of the approach for sampling the biologically-relevant conformational space of TAR was established *a posteriori* by the successful comparison of calculated and experimental RDCs[40] and order parameter S^2 values,[39] as well as by the consistency of our findings with fluorescence experiments[25] and with NMR-based structural information (Tab. S1).[13–21] To the best of our knowledge this represents the first documented instance where such a broad range of TAR experimental data

is successfully reproduced by a single set of unbiased MD simulations. Our calculations are consistent with the NMR-based observations that indicate that: (i) Bending and twisting motions of the upper stem, as well as more local motions, occur spontaneously;[13–21] (ii) The structure samples a wide range of inter-helical angles as the upper stem experiences nearly unrestrained motions at intermediate (sub-μs) rates.[41,42] Once fully validated, the numerical approach is used to re-examine the detailed TAR intrinsic dynamics and explore its functionally-oriented character.

METHODS

The simulations of TAR in aqueous solution described herein have been performed following a published protocol.[39] The initial structures corresponded to the *apo* form (PDB ID: 1ANR)[14] and the complex with the cyclo-RVRTRKGRRIRIPP cyclic peptide (L-22, PDB ID: 2KDQ)[29] depleted of the ligand. The starting structures were chosen on the basis of the RMSD from the average structure and of the agreement with experimental residual dipolar coupling (RDC) values.[40] The systems were embedded into truncated octahedrons containing about 13,000 water molecules. Periodic boundary conditions were applied. The solutes and their images were located at a minimum distance of 2.4 nm. The use of large simulation boxes (395–414 nm^3) was necessary to eliminate artificial interactions between highly charged molecules at the periodically repeated images.[43] Ions were added to reproduce the experimental ion concentration used for NMR structures (50 mM NaCl and 10 mM KCl for the *apo* and the L-22 bound structure, respectively[14,29]). Thus, 40 Na^+ and 12 Cl^- ions and 30 K^+ and 2 Cl^- ions were added to the *apo* and L-22 bound forms of TAR, respectively. A third condition was prepared by adding 30 K^+ and 2 Cl^- ions to the *apo* TAR structure. The parmbsc0 AMBER[37], the TIP3P model[44] and Smith and Dang's force fields[45] were used for RNA, water and the ions, respectively. The Particle Mesh Ewald method[46] was used to treat long-range electrostatic interactions with a real space cutoff of 1.2 nm. The simulations were performed using the program GROMACS 4.5.5[47] with a simulation step of 2 fs. The LINCS algorithm[48] was applied to constrain all bonds involving hydrogen atoms. NPT conditions were achieved by coupling the systems to a Nosè-Hoover thermostat[49] at 300 K and a Andersen-Parrinello-Rahman Barostat[50,51] at 1 atm. The same cutoff was also used for the van der Waals interactions. The subdivision of TAR in quasi-rigid domains (QRDs) followed the structure quasi-rigid domain decomposition method (PiSQRD) of ref[52,53]. The two highly mobile terminal nucleotides were excluded from analysis. RDCs were calculated by applying the Prediction of ALignmEnt from Structure (PALES)[54] program onto 10,000 MD snapshots and by averaging the results.

RESULTS AND DISCUSSION

We ran four independent, 1 μs-long atomistic MD simulations starting from different initial conditions. Two simulations (TAR50a and TAR50b hereafter), differing only for the initial velocities, were based on the NMR *apo* TAR structure at the same ionic strength of the NMR experiments (50 mM NaCl).[14] A third simulation (TAR10a) was based on the NMR TAR structure bound to the cyclic peptide T-22 depleted of the ligand at the ionic strength of NMR experiment (10 mM KCl).[29] The last simulation (TAR10b) were based on the NMR *apo* TAR structure,[14] but with a lower ionic strength than that of experiment (10 mM KCl).

To assess the convergence of the simulated trajectories we considered their projections on the top essential dynamical spaces obtained from a standard covariance analysis. Following Hess's criterion,[55] these projections were next compared with those expected for a random reference. The observed negligible overlap (see Table S2) confirms *a posteriori* adequate sampling of TAR conformations around the equilibrium position. The root-mean-square-deviation (RMSD) from the initial conformations after the first 0.1 μs oscillates between 0.4–0.7 nm (Fig. S3). This RMSD value is compatible with those reported for TAR conformers calculated from replica exchange techniques,[38] which can sample conformational space very effectively, but without providing kinetic information. The good match of RMSD values between the two methods demonstrates that coverage of the conformational space accessible to TAR achieved by retaining the full dynamic detail of MD simulations is exhaustive.

The accuracy of the simulations was established by confronting the calculated RDC40,[a] and order parameter S^2 values with those measured experimentally.[39] The Pearson's correlation coefficients (CCs) between calculated and experimental RDCs are 0.9 (Fig. 2A). To the best of our knowledge, this is the first time that such good agreement is achieved between RDCs extracted from MD simulations of RNA and experimental results.[b] The order parameter S^2 values are also in fair agreement with the experimental data (Fig. 2B). Both techniques confirm that the bulge and the loop in both NMR experiments and computations are the most mobile regions.

The results of Fig. 2 indicate that the four simulations provide similar results, and the same is true for all of the properties calculated in this manuscript. From now on, we report only the result of one simulation based on the *apo* TAR at 50 mM NaCl (TAR50a). The results of the other three simulations are summarized in the SI.

In order to characterize the large-scale motions of TAR, we find it convenient to identify QRDs, which are approximately rigid, although not static. These are derived by an analysis of the fluctuations of all pairwise nucleotide distances.[52,53] QRDs correspond to regions whose internal geometry is largely fixed (resulting in constant modules of pairwise nucleotide distances) while the relative inter-domain position and orientation changes significantly.

The analysis of the simulation indicates that TAR can be subdivided into four QRDs: the apical loop, the bulge and the upper and lower stems (Fig. 3A). The internal quasi-rigid character (i.e. the highly coordinated motions) of the bulge and apical loop has not been noted before, while that of the helical stems would have been expected *a priori* based on the structural and dynamics characteristics of helical regions.[25,42]

[a]The experiments are performed on a TAR mutant, which differs from wild-type TAR by the absence of two nucleotides in the apical loop (E0-TAR, Fig. S4).[40] This does not affect significantly the RDCs relatively to the wild type.[56]

[b]The RDC values were measured at 15 mM sodium phosphate and 25 mM sodium sulfate.[40] However, it has been experimentally observed that changes in ionic strength in the range of the simulations reported here do not greatly affect RDCs.[57] This is also the case for the calculated RDCs: the values predicted here for the simulations at 50 mM NaCl and the 10 mM KCl are very similar (Fig. S8).

The RMSDs of the upper and lower stems and of the bulge QRDs oscillate between 0.2 and 0.4 nm after a few ns (Fig. S3). The RMSDs of the apical loop QRD indicated a less stable simulation - as confirmed by the root-mean-fluctuations (RMSF, Fig. S5) - and oscillate between 0.2 and 0.5 nm. The motion of the lower stem QRD is correlated with that of the bulge; the motion of the lower and upper stems is anti-correlated with that of the loop, while that of the bulge is anti-correlated with that of the upper stem. The motion of the bulge is anti-correlated to that of the apical loop. In particular, the scissor-like motion of the apical loop relative to the bulge results in a canting of the major groove of TAR in the proximity of the bulge (see Fig. 3C). Bulge rearrangements - monitored as in ref.[28] by using the base distance between A22 and U23 - occurs in the hundreds of nanosecond time scale (Fig. S6). Moreover, the correlation plots between the A22-U23 base distance and Ω_{ISB} show three distinct clusters at both ionic strength (Fig. S7), in agreement with simulations in ref.[28].

TAR stems experience transient small amplitude motions [inter stems bending angle (Ω_{ISB}) amplitude < 18°], which occur on a time scale of 1–2 ns, and larger amplitude motions, which occur on the near-μs time scale (Fig. 4A). The overall helical bending motions comprise Ω_{ISB} values between 40° and 130°, which correspond to conformations within the same range of deposited structure[14] (see SI). Ω_{ISB} stabilizes around average values ($<\Omega_{ISB}>$) of ca. 73° for the first 0.15 μs, then decrease to $<\Omega_{ISB}>$ values of ca. 62° (transition amplitude ca. 11°), and finally pass to ca. 92° after ca. 0.36 μs comprising a movement of ca. 20° (Fig. 4A). These observations are consistent with ssNMR data,[42] which suggest that: (i) the stem's motions feature small amplitudes base librations in the ns time scale and larger helical twisting and bending in the ns-μs time scale;[42] (ii) the amplitude of such bending transitions is 13°;[42] (iii) large transitions occur in ca. 700 ns time scale. Our simulations however differ from conclusions from solution NMR,[22,58] as discussed in detail in Tab. S3.

Interestingly, in the case of TAR50a and TAR50b simulations, the two trajectories appear to stabilize at inter stem bending values of ca. 62, 73 and 92° (Fig. S12 and S13). In the case of TAR10a and TAR10b, we mainly observed three states comprising Ω_{ISB} values around ca. 70–71, 84 and 96–97° (Fig. S12 and S13). Thus Ω_{ISB} angle increases with decreasing ionic strength. Accordingly, it was experimentally observed that decreasing the ionic concentration led to a continuous increase in the average inter-helical bend angle.[57] Nevertheless, care should be taken when comparing the set of simulations run at 10 mM KCl with experimental NMR structures; since the only available *apo* TAR structure was determined at 50 mM NaCl ionic strength[14] only the simulations run at the same conditions can be directly compared.

The terminal nucleotides, the bulge (NTs 23–25) and loop residues (NTs 30–36) are the most mobile regions of TAR (Fig. 4B and S5). U38 fluctuates less than U23, which in turn fluctuates less than U25 (Fig. 4B). This order is fully consistent with the ssNMR data.[59] In the simulations, U23 experiences a large-amplitude intermediate-time scale (hundreds of ns) hopping motion and occupies four distinct conformational states [characterized by base glycosidic angles (χ = O4'-C1'-N1-C2 torsional angle) of ca. −165, −125, −75, and +50° (Fig. 4C and S16–18, left panels)]. U23 further experiences a rapid (few ns) small-amplitude twisting of the base plane of the glycosidic bond. These conclusions are consistent with the ssNMR results.[42] In the ssNMR experiments, U25 experiences a motion of the backbone

away from the intra-helical conformation and a μs time scale large-amplitude twisting of the base.[42] In our simulations, U25 exchanges between three distinct angular states (χ ca. −130, −60, and +50°, Fig. 4C and S16–18, central panels) on a time scale of tens-hundreds of ns, in fair agreement with ssNMR.[42] Finally, U38 shows experimentally small-amplitude local motions at a much faster rate with respect to helical motion (ns time scale).[42] U38 forms H-bonds with A27, and it is also stacked between C37 and C39 for all the simulation time. Moreover, the U38 glycosidic angle populates one single state (χ ca. 160°) with limited motions in the ns timescale (Fig. 4C and Figs. S16–18, right panels). This is fully consistent with the ssNMR data, which shows that U38 experiences small-amplitude local motions at a much faster rate with respect to helical motion (ns time scale).[42] In conclusion, our results are in good agreement with ssNMR data collected on samples singly labelled at U23, U25 and U38.

The comparison with the simulations in ref.[28] is necessarily limited to RDCs, and cannot be extended to all of the available NMR data on TAR (including order parameters S^2 and time scale of motion of nucleotides) that are only reported in the present study. There are two available RDC's data sets, measured in different conditions. The first data set is measured in aqueous solution,[40] consistent with our simulations. The RDCs of the second data set[28] are measured using an orienting medium of TAR variants with elongated stems,[c] whose structural and dynamics properties may be different from those of native TAR in aqueous solutions. Comparing calculated RDC's values with the data from ref.[40] (Fig. 2 and S19) is more meaningful than a comparison with the data of ref.[28]. Although the latter authors do not report quantitative measures of the correlation between experimental and predicted RDC's (e.g. correlation coefficients), visual inspection of the correlation plots indicates that our predictions are more accurate.

CONCLUDING REMARKS

RNA's functional complexity is rooted not only in its intricate 3D structure but also depends on its dynamics. Motions in RNA indeed range from local changes in base-pairing to large-scale collective bending and twisting of helical domain, all of which occur over a range of timescales.[4] The complex multilayer dynamics of TAR was here addressed by means of four microsecond-long MD simulations with the new AMBER force field. Several order parameters, previously measured in NMR experiments, are quantitatively reproduced with unprecedented agreement by the simulations. Building on the accord between computation and experiment, we investigated the unresolved issue of the typical timescale governing large-scale motions in TAR. On the one hand, the calculations support unambiguously the conclusion that dynamics occurs in the ns-μs time scale (consistent with ssNMR studies), a rate compatible with RNA-ligand binding processes.[4] This shows that the associated internal dynamics has a functionally-oriented character. On the other hand, by using a suitable multiscale analysis, we conclude that conformational exchange processes relevant to ligand binding (namely transitions between the *apo* and *holo* forms) occur in the near-μs time scale.

[c]These are: a non-elongated construct with the loop shortened, two constructs in which either the lower or the upper stem is elongated by 22 base pairs and a shortened loop, and finally one construct in which the lower stem is elongated by three base pairs and a shortened loop.

This conclusion is consistent with the findings of ssNMR measurements[41,42,59] that indicate a key role of stochastic hinge-bending motion of TAR occurring in the hundreds of ns time scale for inducing a conformation conducive to Tat binding. The current atomistic simulations extend significantly the insight offered by NMR by elucidating, with unprecedented structural detail, the innate internal dynamics of TAR and its functionally-oriented implications.

Supplementary Material

Refer to Web version on PubMed Central for supplementary material.

Acknowledgments

This work has been supported with grants from the Project ISS UPR- 20009-1301355 (CUP I85J08000040005) and from the Italian Ministry of Education, PRIN 2010HXAW77. FM was financed by Programma Operativo del Fondo Sociale Europeo 2007/2013 of Regione Autonoma Friuli Venezia Giulia and by CIRMMP (Consorzio Interuniversitario di Risonanze Magnetiche di Metallo-Proteine). Work at the University of Washington is supported by a grant from NSF. This project was granted 190,000 core hours on the JUROPA supercomputer in the Jülich Supercomputing Centre through the NIC program (NIC: 6593).

References

1. Breaker RR. Mol. Cell. 2011; 43:867. [PubMed: 21925376]
2. Aalto AP, Pasquinelli AE. Curr. Opin. Cell Biol. 2012; 24:333. [PubMed: 22464106]
3. Serganov A, Patel DJ. Curr. Opin. Struct. Biol. 2012; 22:279. [PubMed: 22579413]
4. Al-Hashimi HM, Walter NG. Curr. Opin. Struct. Biol. 2008; 18:321. [PubMed: 18547802]
5. Muesing MA, Smith DH, Capon DJ. Cell. 1987; 48:691. [PubMed: 3643816]
6. Frankel AD. Curr. Opin. Genet. Dev. 1992; 2:293. [PubMed: 1638124]
7. Weeks KM, Ampe C, Schultz SC, Steitz TA, Crothers DM. Science. 1990; 249:1281. [PubMed: 2205002]
8. Churcher MJ, Lamont C, Hamy F, Dingwall C, Green SM, Lowe AD, Butler PJG, Gait MJ, Karn J. J. Mol. Biol. 1993; 230:90. [PubMed: 8450553]
9. Huang W, Varani G, Drobny GP. J. Am. Chem. Soc. 2010; 132:17643. [PubMed: 21105680]
10. Wang Y, Liu X-Y, De Clercq E. Mini Rev. Med. Chem. 2009; 9:379. [PubMed: 19275730]
11. Kikuta E, Aoki S, Kimura E. J. Am. Chem. Soc. 2001; 123:7911. [PubMed: 11493067]
12. Sztuba-Solinska J, Shenoy SR, Gareiss P, Krumpe LRH, Le Grice SFJ, O'Keefe BR, Schneekloth JS. J. Am. Chem. Soc. 2014; 136:8402. [PubMed: 24820959]
13. Aboul-ela F, Karn J, Varani G. J. Mol. Biol. 1995; 253:313. [PubMed: 7563092]
14. Aboul-Ela F, Karn J, Varani G. Nucleic Acids Res. 1996; 24:3974. [PubMed: 8918800]
15. Faber C, Sticht H, Schweimer K, Rosch P. J. Biol. Chem. 2000; 275:20660. [PubMed: 10747964]
16. Du Z, Lind KE, James TL. Chem. Biol. 2002; 9:707. [PubMed: 12079782]
17. Murchie AI, Davis B, Isel C, Afshar M, Drysdale MJ, Bower J, Potter AJ, Starkey ID, Swarbrick TM, Mirza S, Prescott CD, Vaglio P, Aboul-ela F, Karn J. J. Mol. Biol. 2004; 336:625. [PubMed: 15095977]
18. Davis B, Afshar M, Varani G, Murchie AI, Karn J, Lentzen G, Drysdale M, Bower J, Potter AJ, Starkey ID, Swarbrick T, Aboul-ela F. J. Mol. Biol. 2004; 336:343. [PubMed: 14757049]
19. Davidson A, Leeper TC, Athanassiou Z, Patora-Komisarska K, Karn J, Robinson JA, Varani G. Proc. Natl. Acad. Sci. USA. 2009; 106:11931. [PubMed: 19584251]
20. Davidson A, Patora-Komisarska K, Robinson JA, Varani G. Nucleic Acids Res. 2011; 39:248. [PubMed: 20724442]
21. Davidson A, Begley DW, Lau C, Varani G. J. Mol. Biol. 2011; 410:984. [PubMed: 21763501]

22. Zhang Q, Stelzer AC, Fisher CK, Al-Hashimi HM. Nature. 2007; 450:1263. [PubMed: 18097416]
23. Calnan B, Tidor B, Biancalana S, Hudson D, Frankel A. Science. 1991; 252:1167. [PubMed: 1709522]
24. Karn J. J. Mol. Biol. 1999; 293:235. [PubMed: 10550206]
25. Lu J, Kadakkuzha BM, Zhao L, Fan M, Qi X, Xia T. Biochemistry. 2011; 50:5042. [PubMed: 21553929]
26. Edwards TE, Okonogi TM, Robinson BH, Sigurdsson ST. J. Am. Chem. Soc. 2001; 123:1527. [PubMed: 11456739]
27. Bailor MH, Sun X, Al-Hashimi HM. Science. 2010; 327:202. [PubMed: 20056889]
28. Salmon L, Bascom G, Andricioaei I, Al-Hashimi HM. J. Am. Chem. Soc. 2013; 135:5457. [PubMed: 23473378]
29. Bardaro MF Jr, Shajani Z, Patora-Komisarska K, Robinson JA, Varani G. Nucleic Acids Res. 2009; 37:1529. [PubMed: 19139066]
30. Denning EJ, Priyakumar UD, Nilsson L, Mackerell AD Jr. J. Comput. Chem. 2011; 32:1929. [PubMed: 21469161]
31. Foloppe N, MacKerell JAD. J. Comput. Chem. 2000; 21:86.
32. MacKerell AD, Banavali NK. J. Comput. Chem. 2000; 21:105.
33. Sponer J, Spacková Na. METHODS. 2007; 43:278. [PubMed: 17967698]
34. Sponer J, Cang X, Cheatham TE. METHODS. 2012; 57:25. [PubMed: 22525788]
35. Banáš P, Hollas D, Zgarbová M, Jurečka P, Orozco M, Cheatham TE, Šponer Ji, Otyepka M. J. Chem. Theory Comput. 2010; 6:3836.
36. Besseova I, Otyepka M, Reblova K, Sponer J. Phys. Chem. Chem. Phys. 2009; 11:10701. [PubMed: 20145814]
37. Perez A, Marchan I, Svozil D, Sponer J, Cheatham TE 3rd, Laughton CA, Orozco M. Biophys. J. 2007; 92:3817. [PubMed: 17351000]
38. Fulle S, Christ NA, Kestner E, Gohlke H. J. Chem. Inf. Model. 2010; 50:1489. [PubMed: 20726603]
39. Do TN, Ippoliti E, Carloni P, Varani G, Parrinello M. J. Chem. Theory Comput. 2012; 8:688. [PubMed: 26596616]
40. Zhang Q, Throolin R, Pitt SW, Serganov A, Al-Hashimi HM. J. Am. Chem. Soc. 2003; 125:10530. [PubMed: 12940730]
41. Emani PS, Olsen GL, Varani G, Drobny GP. J. Phys. Chem. A. 2011; 115:12055. [PubMed: 21870804]
42. Olsen GL, Bardaro MF Jr, Echodu DC, Drobny GP, Varani G. J. Am. Chem. Soc. 2010; 132:303. [PubMed: 19994901]
43. Pérez A, Luque FJ, Orozco M. Acc. Chem. Res. 2012; 45:196. [PubMed: 21830782]
44. Jorgensen WL, Chandrasekhar J, Madura JD, Impey RW, Klein ML. J. Chem. Phys. 1983; 79:926.
45. Smith DE, Dang LX. J. Chem. Phys. 1994; 100:3757.
46. Essmann U, Perera L, Berkowitz ML, Darden T, Lee H, Pedersen LG. J. Chem. Phys. 1995; 103:8577.
47. Pronk S, Páll S, Schulz R, Larsson P, Bjelkmar P, Apostolov R, Shirts MR, Smith JC, Kasson PM, van der Spoel D, Hess B, Lindahl E. Bioinformatics. 2013; 29:845. [PubMed: 23407358]
48. Van Der Spoel D, Lindahl E, Hess B, Groenhof G, Mark AE, Berendsen HJ. J. Comput. Chem. 2005; 26:1701. [PubMed: 16211538]
49. Nosé S, Klein ML. Mol. Phys. 1983; 50:1055.
50. Andersen HC. J. Chem. Phys. 1980; 72:2384.
51. Parrinello M, Rahman A. J. Appl. Phys. 1981; 52:7182.
52. Aleksiev T, Potestio R, Pontiggia F, Cozzini S, Micheletti C. Bioinformatics. 2009; 25:2743. [PubMed: 19696046]
53. Potestio R, Pontiggia F, Micheletti C. Biophys. J. 2009; 96:4993. [PubMed: 19527659]
54. Zweckstetter M, Bax A. J. Am. Chem. Soc. 2000; 122:3791.

55. Hess B. Phys. Rev. E. 2002; 65:031910.
56. Dethoff EA, Hansen AL, Musselman C, Watt ED, Andricioaei I, Al-Hashimi HM. Biophys. J. 2008; 95:3906. [PubMed: 18621815]
57. Casiano-Negroni A, Sun X, Al-Hashimi HM. Biochemistry. 2007; 46:6525. [PubMed: 17488097]
58. Zhang Q, Sun X, Watt ED, Al-Hashimi HM. Science. 2006; 311:653. [PubMed: 16456078]
59. Olsen GL, Echodu DC, Shajani Z, Bardaro MF, Varani G, Drobny GP. J. Am. Chem. Soc. 2008; 130:2896. [PubMed: 18275190]

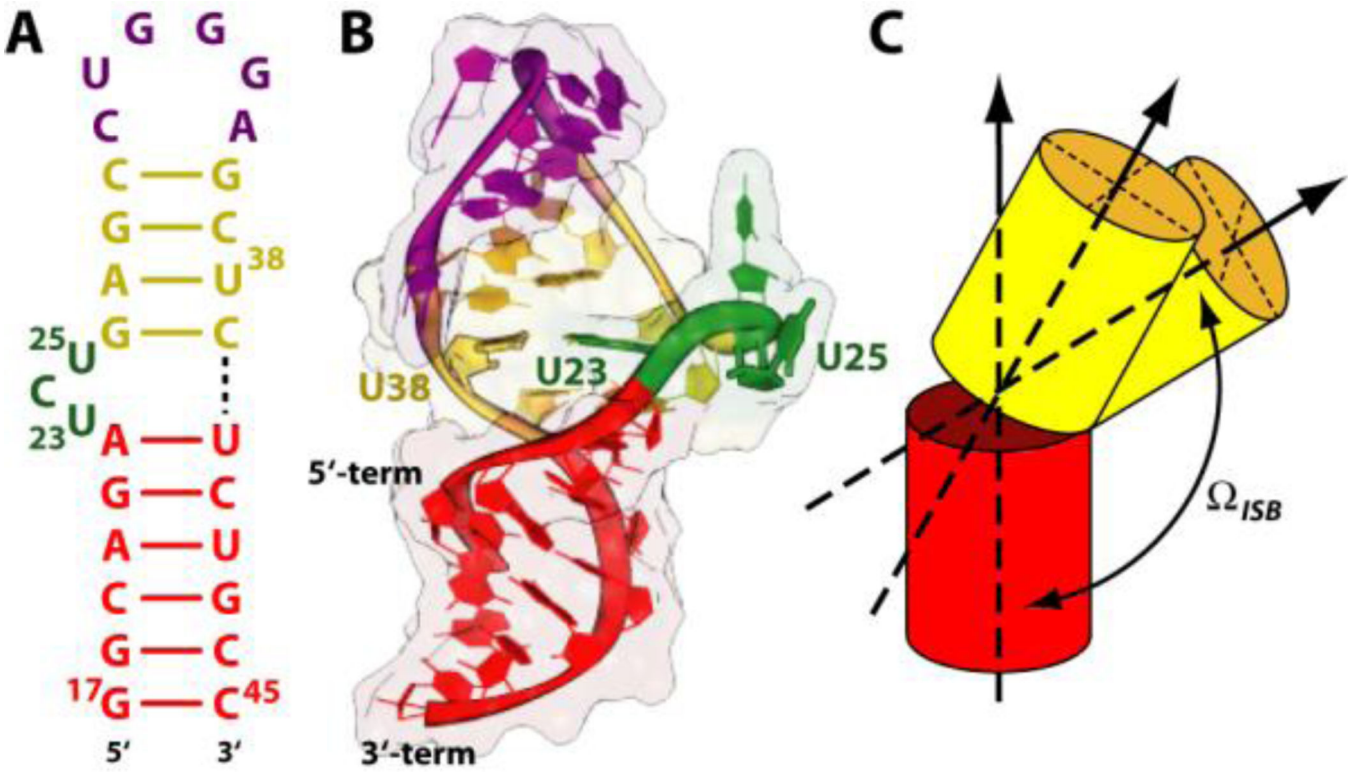

Figure 1.

HIV-1 TAR. Sequence (**A**) and cartoon representation (**B**) of the structure obtained from NMR studies.[29] The apical loop, bulge and the upper and lower stems are colored in magenta, green, yellow and red, respectively. (**C**) Cartoon representation of the inter-stem bending (Ω_{ISB}) angle involved in the movements of the helical stems movement. See Fig. S2 in the Supplementary Information for further details.

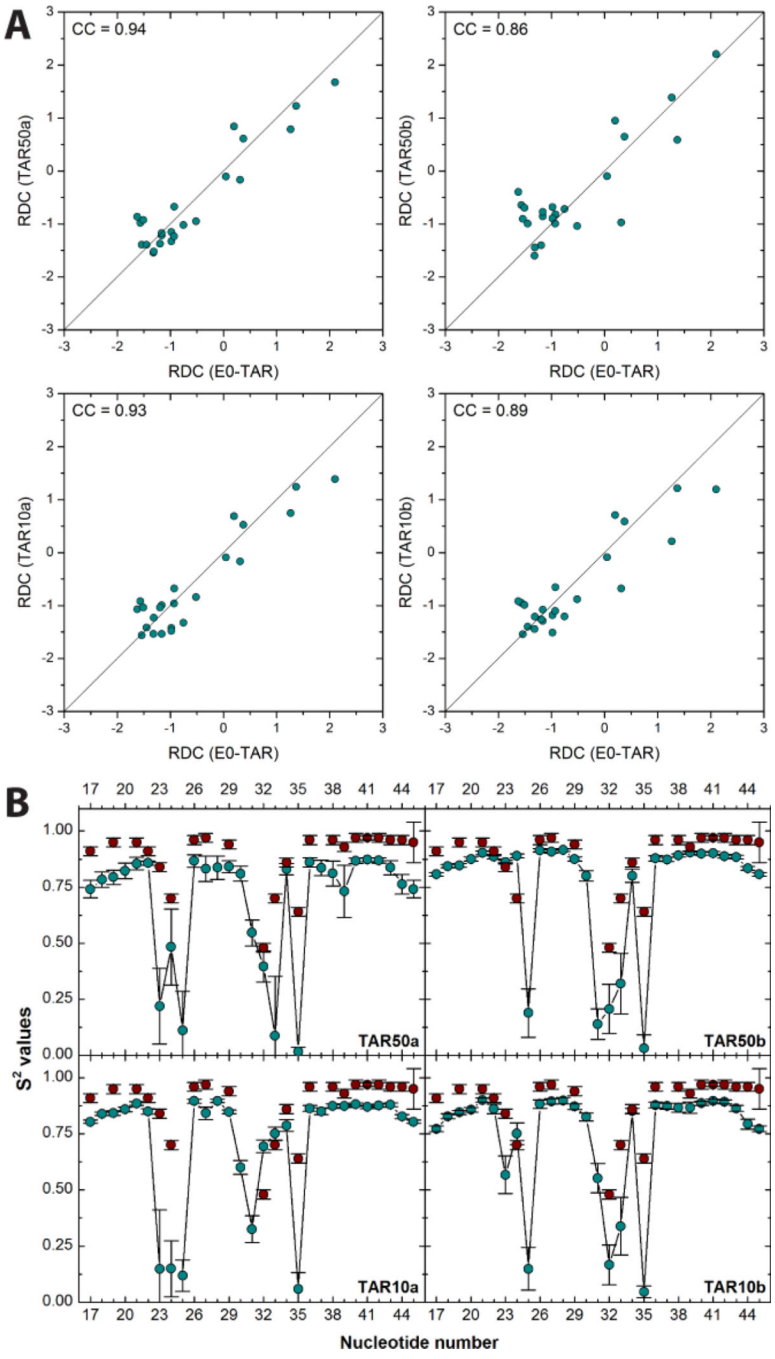

Figure 2.

Comparison between NMR data of TAR and four independent, μs-long MD simulations (TAR50a, TAR50b, TAR10a and TAR10b). (**A**) Correlation plots of experimental RDCs (Hz) from E0-TAR[40] and the corresponding calculated values. (**B**) Calculated (blue circles) and experimental[39] (red circles) order parameter (S^2, arbitrary units) values for nucleotides 17–45 of TAR.

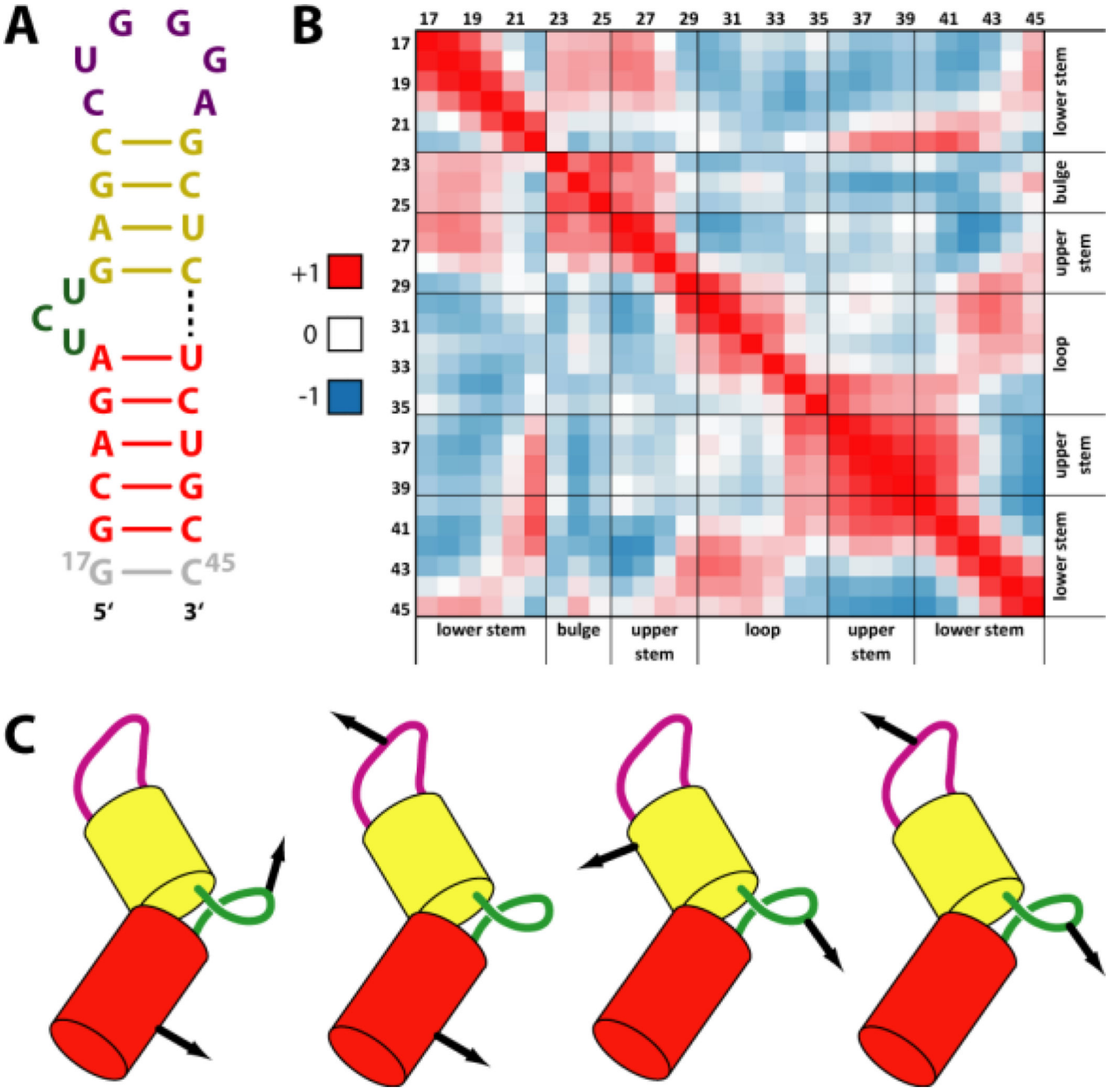

Figure 3.

Quasi-rigid domains (QRDs) of TAR. (**A**) Calculated QRDs emerging from the MD simulations of TAR50a; additional details can be found in Fig. S9 of supporting information. (**B**) Residue-by-residue map of correlation matrices for the C4’ atoms of TAR. Red and dark blue regions refer to correlated and anti-correlated movements, respectively. (**C**) Cartoon representation of correlated and anti-correlated motions of QRDs.

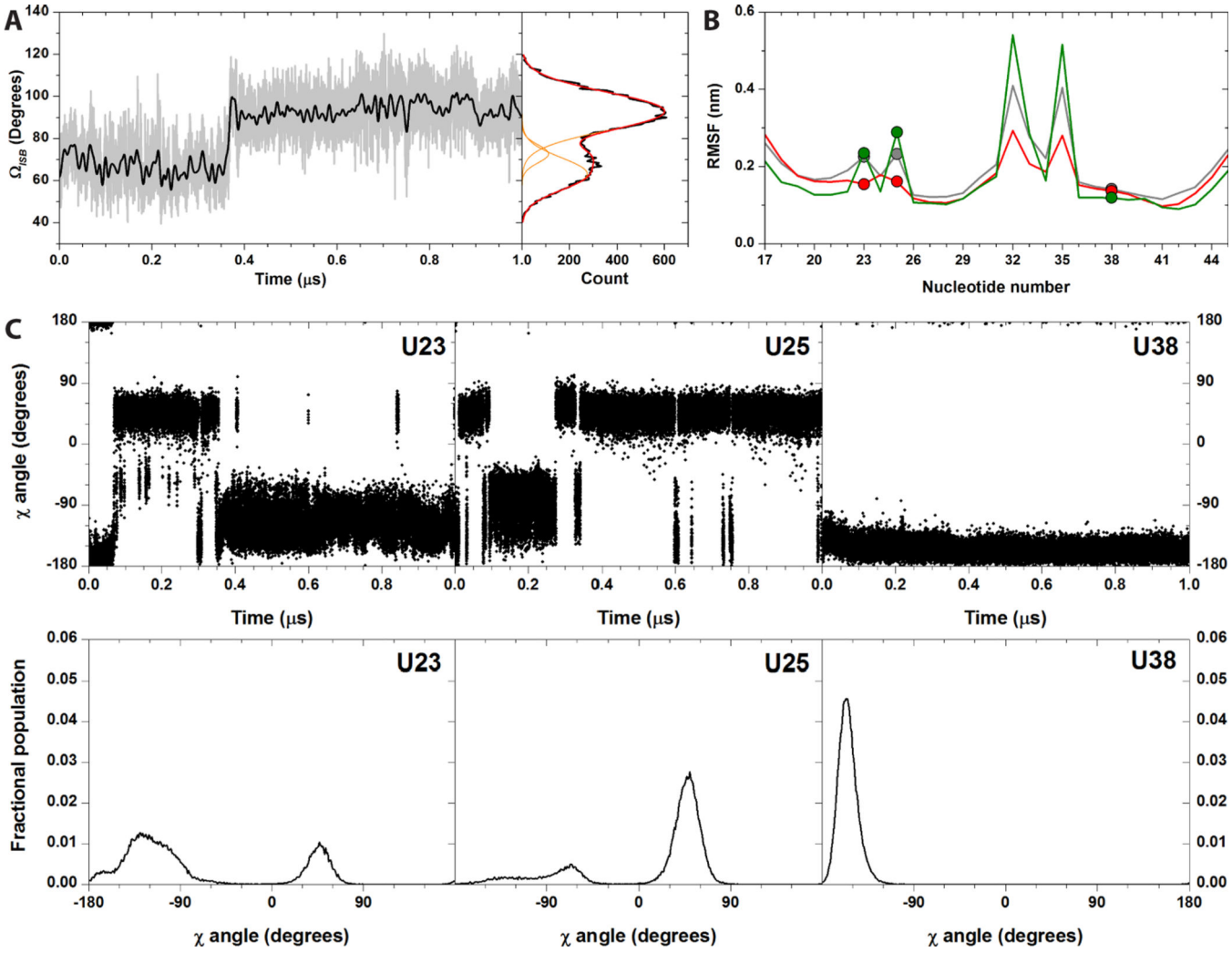

Figure 4.

Selected properties from the TAR50a MD simulation. (**A**) Ω_{ISB} values plotted *vs.* simulation time (grey line). The black line is obtained by applying a Fast Fourier Transform filter in order to reduce the noise in the data. The right panel reports the distribution of the calculated Ω_{ISB} angle values (black line). The Gaussian curves used to fit the Ω_{ISB} distribution are in orange, while the sum of the fitting Gaussians is in red. (**B**) Calculated RMSFs values of each nucleotide atoms (grey), of the C4' atoms of each nucleotide (red) and of C5 atoms of each nucleotide (green). RMSF values of U23, U25, and U38 are highlighted by dots in each curve. (**C**) Time evolution (upper panels) and distribution (bottom panels) of the χ torsional angle of U23, U25 and U38, as observed in the MD simulation TAR50a. Correspondent plots for the TAR50b, TAR10a, and TAR10b simulations are reported in the SI.